Anatomy of Dzyaloshinskii-Moriya Interaction at Co/Pt Interfaces

Hongxin Yang,[1,2] André Thiaville,[2] Stanislas Rohart,[2] Albert Fert,[3] and Mairbek Chshiev[1]
[1]Univ. Grenoble Alpes, INAC-SPINTEC, 38000 Grenoble, France; CNRS, SPINTEC, 38000 Grenoble, France; and CEA, INAC-SPINTEC, 38000 Grenoble, France
[2]Laboratoire de Physique des Solides, Université Paris-Sud, CNRS UMR 8502, 91405 Orsay Cedex, France
[3]Unité Mixte de Physique CNRS/Thales, 1 Avenue Fresnel, 91767 Palaiseau, France and Université Paris-Sud, 91405 Orsay, France
(Received 2 April 2015; published 30 December 2015)

The Dzyaloshinskii-Moriya interaction (DMI) has been recently recognized to play a crucial role in allowing fast domain wall dynamics driven by spin-orbit torques and the generation of magnetic Skyrmions. Here, we unveil the main features and microscopic mechanisms of DMI in Co/Pt bilayers via first principles calculations. We find that the large DMI of the bilayers has a dominant contribution from the spins of the interfacial Co layer. This DMI between the interfacical Co spins extends very weakly away from the interface and is associated with a spin-orbit coupling in the adjacent atomic layer of Pt. Furthermore, no direct correlation is found between DMI and proximity induced magnetism in Pt. These results clarify the underlying mechanisms of DMI at interfaces between ferromagnetic and heavy metals and should help optimizing material combinations for domain wall and Skyrmion-based devices.

DOI: 10.1103/PhysRevLett.115.267210 PACS numbers: 75.70.Cn, 71.15.Mb, 73.43.Cd

The discovery of fast current-controlled domain wall motion induced by spin-orbit torques in perpendicularly magnetized thin ferromagnetic layers deposited on nonmagnetic metals of large spin-orbit coupling (SOC) [1] is promising for the development of novel memory and storage devices with high density, performance, and endurance [2]. The origin of the current-controlled DW motion was first attributed to the Rashba effect [1,3–5] and later to the spin Hall effect (SHE) [6,7]. In 2012 it was shown by micromagnetic calculations [8], and later confirmed experimentally [9,10], that the role of Dzyaloshinskii-Moriya interaction (DMI) [11–13] at interfaces between ferromagnetic (FM) and heavy nonmagnetic (NM) metals [14–18] was essential to stabilize the DWs in a Néel configuration with a given chirality, allowing their fast motion by SHE in a direction fixed by this chirality. DMI also stabilizes magnetic Skyrmions in magnetic thin films deposited on heavy metals [19–25]. Measurements of interfacial DMI, initially based on DWs [26–32], were recently expanded by spin-wave spectroscopy [33–35]. Put together, the measured DMI values reveal a large sensitivity to both materials and interface structure. An in-depth understanding of interfacial DMI is therefore in need. Several schemes have been proposed to compute interfacial DMI by *ab initio* techniques [18,36,37]. But a simple physical picture of interfacial DMI is still elusive, with several fundamental questions to clear up: how does the DMI extend away from the interface? Where is the corresponding electronic energy source located? Is the existence of a proximity-induced magnetization in the nonmagnetic layer important?

In this Letter, we evaluate and analyze in depth, from first principles calculations, the DMI behavior at Co/Pt and related FM/NM bilayers. The Co/Pt interface is a natural choice since the largest effects at room temperature were observed in this system [28,31,35,38]. We demonstrate that the predominant DMI is acting on the Co spins in the interface FM atomic layer, with only a weak extension in Co and Pt away from this layer. Furthermore, the SOC energy associated with this predominant DMI is located not in the Co but in the neighbor Pt sites. We also show that the existence of proximity-induced magnetization on the interface sites of heavy NM metal is not essential for the DMI, and that interface intermixing has a damaging impact on the DMI strength.

We use *ab initio* calculations on Co/Pt bilayers to evaluate both the total DMI of the bilayer and its distribution in the successive atomic layers of Co and Pt. The DMI energy between normalized spins, restricted to nearest neighbors (as justified *a posteriori*), can be written as

$$E_{\mathrm{DMI}} = \sum_{\langle i,j \rangle} \mathbf{d}_{ij} \cdot (\mathbf{S}_i \times \mathbf{S}_j), \tag{1}$$

with summation over bonds involving DMI vectors $\mathbf{d}_{ij}$ for two types of pairs, those inside a given layer k, and interlayer pairs between a layer k and layers above or below. It turns out that the contributions from interlayer pairs are very small (see Supplemental Material S1 [39]), so that, in first approximation, we will neglect them. From the Moriya symmetry rules [12], the DMI vector for the layer k can be written as $\mathbf{d}_{ij}^{k} = d^{k}(\hat{\mathbf{z}} \times \hat{\mathbf{u}}_{ij})$ (see Supplemental Material S1 [39]), where $\hat{\mathbf{z}}$ and $\hat{\mathbf{u}}_{ij}$ are unit vectors pointing along z and from site i to site j, respectively. The total DMI strength, d^{tot} (expected to be close to $\sum_k d^k$ as it will be confirmed in the following), is derived (see Supplemental Material S1 [39]) by identifying

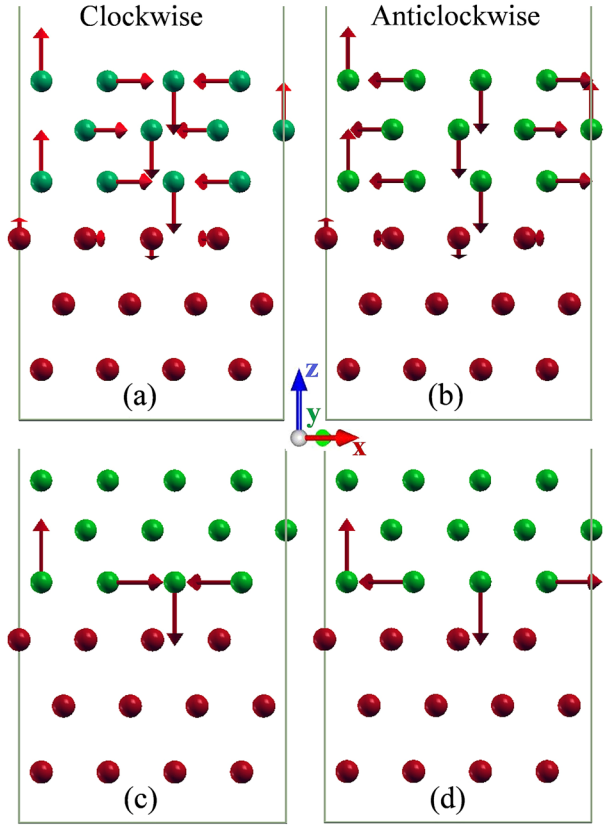

FIG. 1 (color online). Examples of (a),(c) clockwise (CW) and (b),(d) anticlockwise (ACW) spin configurations used to calculate the DMI of hcp(0001)Co/fcc(111)Pt bilayers. The total d^{tot} and the layer-resolved d^{k} DMI parameters were found using (a), (b) and (c),(d) spiral configurations, respectively (see the text). Green and red correspond respectively to Co and Pt. Spin moments of Pt atoms are multiplied by 10 for convenience. The side view of the Co(3)Pt(3) unit cell is represented.

the difference between the DFT energies E_{CW} and E_{ACW} for opposite chirality spin configurations [as those shown in Figs. 1(a) and 1(b) for a given value of the cycloid wavelength] with the corresponding energy differences calculated from Eq. (1):

$$d^{\mathrm{tot}} = (E_{\mathrm{CW}} - E_{\mathrm{ACW}})/m. \tag{2}$$

The number m depends on the wavelength of the cycloid and, for example, is 12 for the cycloid wavelength of $n = 4$ atomic distances in Fig. 1 (Supplemental Material S3 [39]). The d^{tot} can be seen as the DMI strength concentrated in a single atomic layer and producing an equivalent effect (at least if the total thickness is smaller than the exchange stiffness length). The global effect on the bilayer can also be expressed by the micromagnetic energy per volume unit of the magnetic film [40–42]:

$$E = D\left[m_z \frac{dm_x}{dx} - m_x \frac{dm_z}{dx}\right] + id(x \leftrightarrow y), \tag{3}$$

where the coefficient D is related to d^{tot} by (Supplemental Material S2 and S3 [39])

$$D = \frac{3\sqrt{2}d^{\mathrm{tot}}}{N_F a^2}, \tag{4}$$

in which a is the fcc lattice constant and N_F represents the number of magnetic layers.

The VASP package was employed [43,44] using supercells with 1 to 3 atomic layers (ML) of Co on 1 to 3 ML of nonmagnetic (NM) metals (Fig. 1). In order to extract the DMI vector, calculations were performed in three steps. First, structural relaxations were performed until the forces become smaller than 0.001 eV/Å for determining the most stable interfacial geometries. Next, the Kohn-Sham equations were solved, with no SOC, to find out the charge distribution of the system's ground state. Finally, SOC was included and the self-consistent total energy of the system was determined as a function of the orientation of the magnetic moments which were controlled by using the constrained method implemented in VASP. This method has been used for DMI calculations in bulk spin-frustrated systems and insulating chiral-lattice magnets [36,45], and was adapted here to the case of interfaces. Details of the model are described in the Supplemental Material S1–S3 [39].

Prior to presenting the numerical results, we want to point out that calculations on different values n for the cycloid wavelength give very similar results (within 7%); see the Supplemental Material S3 [39]. Significant DMI for the next nearest neighbor and beyond pairs (NNN) would lead to results depending significantly on the wavelength (one can check that the DMI of NNN would not contribute for $n = 4$ but only for larger n). The very weak dependence on the wavelength (see Supplemental Material S3 [39]) means that the non-nearest pair DMI can be neglected and led us to prefer the simpler analysis with only nearest neighbor DMI coefficients. In Fig. 2 we present results obtained for $n = 4$. For the total DMI strength d^{tot} of hcp(0001)Co/fcc(111)Pt bilayers with different Pt and Co thicknesses, we find large values in the range 1.5–3 meV, of anticlockwise chirality (as defined in Ref. [9]), with a dependence on the thickness of Co and Pt shown in Fig. 2(a). The dependence on Co thickness, as explained by layer-resolved results shown below, comes from the small but not negligible extension of the DMI to other Co layers away from the interface Co layer. Except for the Co (1)Pt(N) series, the influence of the Pt thickness is weak. Globally d^{tot} tends to an approximately constant value at large thickness which is consistent with the interface character of the DMI. D, as it corresponds to an average of the DMI in the Co film, shows the expected decrease with the Co thickness [Fig. 2(b)]. In order to consider more realistic situations, we have also studied the effect of intermixing between Co and Pt. When one Co atom is swapped with Pt at interface (25% interfacial mixing), the

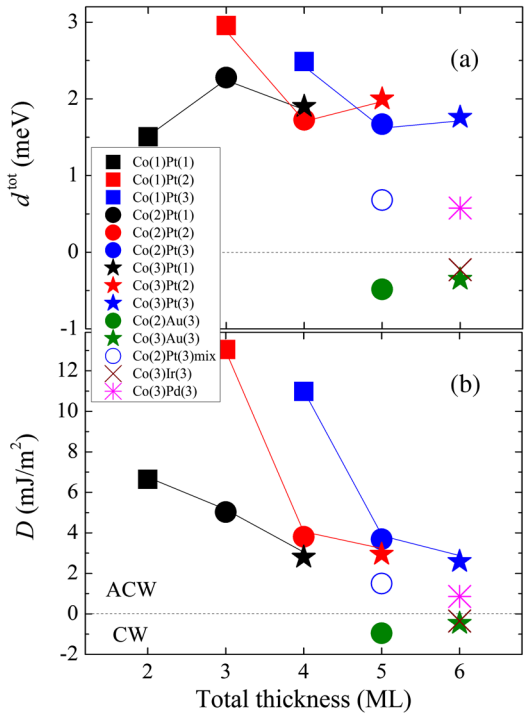

FIG. 2 (color online). (a) Total DMI coefficient d^{tot}. (b) Micromagnetic DMI coefficient D of the Co/Pt, Co/Ir, Co/Au, Co/Pd bilayers, and Co/Pt bilayer with mixed interfaces, as a function of the total number of atomic layers. Solid lines can be used to follow the variation the DMI of Co/Pt bilayers as a function of the Co thickness for a given Pt thickness.

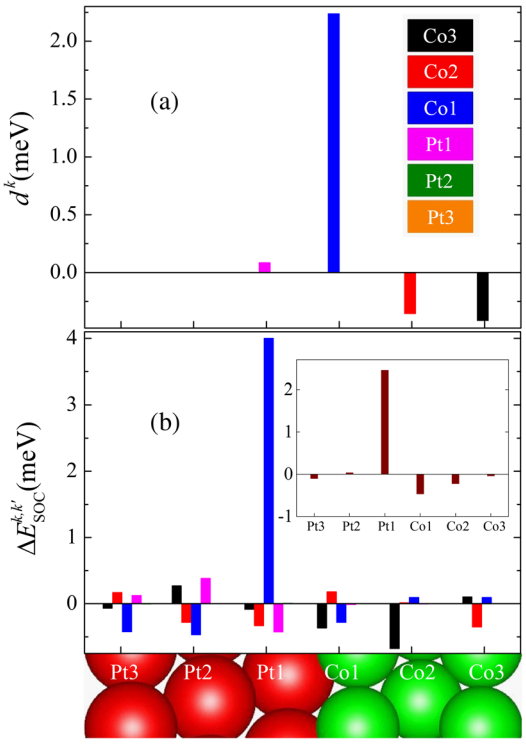

FIG. 3 (color online). Anatomy of DMI for the Co(3)Pt(3) structure. (a) Layer resolved DMI coefficient d^k vs layer k. (b) The corresponding localization of the associated SOC energy source in the atomic sites of all layers k'. For example, the large DMI coefficient d^{Co1} of the spin pairs in the Co1 layer [blue bar in (a)] is associated with a large variation $\triangle E^{Co1,Pt1}_{SOC}$ of the SOC electronic energy in the Pt1 layer [blue bar in (b)] induced by an inversion of the chirality in Co1. For comparison, the distribution of SOC energy variations induced by an inversion of the chirality of the total structure is shown (inset).

total DMI is decreased by half (blue open circles in Fig. 2), twice the amount expected from a naive estimate.

In order to clarify the physics of the interface DMI, we calculated the layer-resolved DMI vector amplitude d^k by considering spin configurations as those of Figs. 1(c) and 1(d) with opposite chirality in a single layer while spins in all other layers are constrained to be along y (Supplemental Material S1. A [39]). The corresponding DFT energies E^k_{CW} and E^k_{ACW} allow finding d^k from Eq. (2). The results for hcp(0001)Co(3ML) on fcc(111)Pt(3ML) are shown in Fig. 3(a). As a test of the accuracy of our approach, we have checked that the sum of the d^k of the different layers is close to d^{tot} with the slight difference ($\sim$10%) caused by the aforementioned interlayer contributions integrated into d^{tot} but not into d^k (Supplemental Material S1 [39]), and by the fact that DFT calculations on differently constrained configurations cannot be strictly equivalent. We will show now that the physics of DMI is cleared up by looking at the distribution of the d^k among the various layers k, and by the spatial origin of each d^k, described by $\triangle E^{k,k'}_{SOC}$ representing the SOC energy difference [46] in the layer k' between spin configurations of opposite chiralities in layer k (Fig. 3).

The most obvious feature of the distribution of d^k in Fig. 3(a) is that the DMI is predominantly located at the interfacial Co layer, as indicated by the blue bar on Co1, with definitely smaller and opposite DMIs in Co2 and Co3, and a much smaller contribution in Pt1 (almost nothing in Pt2 and Pt3). It is interesting to see where the difference between the spin-orbit coupling energies calculated for opposite chiralities in the Co1 layer, i.e., $\triangle E^{Co1,k'}_{SOC}$, is located. As shown in Fig. 3(b), the large DMI between the Co spins at the interface (k = Col) is associated with a large SOC energy change $\triangle E^{Co1,Pt1}_{SOC}$ in the adjacent Pt layer. This is consistent with the Fert-Levy model [13] describing the DMI of a typical noncentrosymmetric Co-Co-Pt triplet as a 3-site interaction in which a change of the chirality of the relative orientation between the Co spins induces a change of the spin-orbit energy on the Pt site. The confusion between the localization of the spins subjected to the strongest DMI and the localization of the corresponding SOC energy source is frequent in recent publications [37]. Considering the Co3 layer, as Co3 is too far from Pt, its small DMI is associated to (small) SOC energy changes in Co2 and Co1. Similarly, the DMI of Co2 takes its origin from both adjacent Co layers and the moderately distant Pt1 and Pt2 layers (red bars). The DMI is very small for the proximity-induced spins (about 0.3 μ_B)

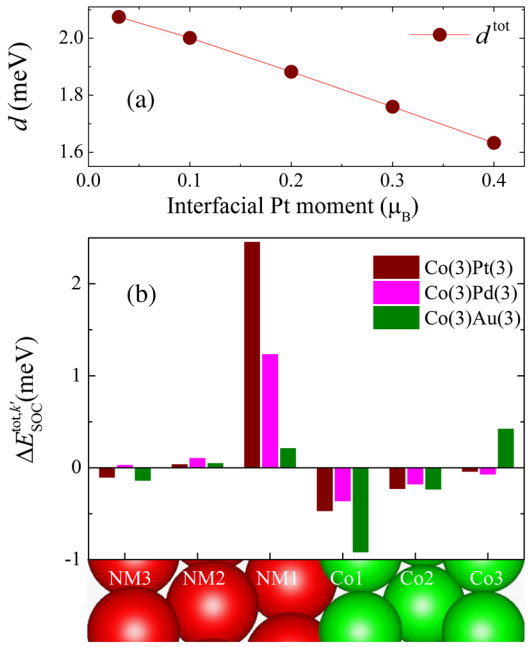

FIG. 4 (color online). Influence of the proximity induced moment on DMI for Co/Pt and localization of $\triangle E_{\mathrm{SOC}}^{\mathrm{tot},k'}$ for Co/Pt, Co/Pd, and Co/Au bilayers. (a) DMI parameter d^{tot} for Co(3)Pt(3) as a function the interfacial spin moment in Pt1 layer. (b) Distribution of SOC energy associated with d^{tot} across Co/Pt, Co/Pd, and Co/Au structures. $\triangle E_{\mathrm{SOC}}^{\mathrm{tot},k'}$ on NM1 sites is strongly reduced in the case of Co/Pd and Co/Au compared to Co/Pt bilayers, resulting in strong reduction of DMI.

in the interfacial Pt1 monolayer with a SOC energy originating mainly from other Pt layers (magenta bars). The SOC energy distribution associated with the total DMI d^{tot}, shown in inset of Fig. 3(b), is very similar to that obtained for d^{Co1}. One also sees that the small DMI of Co2 and Co3 is opposite to the large DMI of Co1, which explains the smaller d^{tot} in Co(2)Pt(3) and Co(3)Pt(3) compared to Co(1)Pt(3) in Fig. 2(a).

It was suggested that DMI at FM/NM interfaces is directly related to the existence of a proximity induced magnetic moment (PIM) in NM [38]. To test this suggestion, we derived the DMI as a function of PIM by constraining the magnitude of the latter in the Pt1 layer of a Pt(3)/Co(3) structure. Actually, as shown in Fig. 4(a), we find the opposite result: a Pt moment reduction increases the DMI, d^{tot}. The DMI is maximum at about zero Pt moment with an almost linear decrease of 31% for d^{tot} when PIM increases from zero to 0.4 μ_B. This behavior can be explained by the competition between the SOC and exchange splitting which reduces the DMI. Furthermore, in spite of a large moment on Pd in Co/Pd that is comparable to that on Pt in Co/Pt, we find a definitely smaller DMI for Co/Pd (Fig. 2), which indicates that the essential factor is the SOC (larger in the Pt 5d states than in the Pd 4d states).

For Co/Pt(111), our DMI values are in agreement with recent theoretical (1.8 meV for Co ML on Pt [24] and 3.5 meV for 3 Co ML on Pt [18]) and experimental [29,35] reports. As a comparison study, we find that, in Co/Au, DMI is much weaker and of opposite chirality compared to that in Co/Pt (cf. Fig. 2). The origin of this difference of DMI between these similar systems can be attributed to the absence of strongly spin-orbit coupled d states at the Fermi level in Au yielding a strong reduction of $\triangle E_{\mathrm{SOC}}^{\mathrm{tot,Au1}}$ on Au1 [Fig. 4(b)]. We have also calculated DMI at Fe/Ir and Co/Ir interfaces. We find a very large clockwise DMI (−1.9 meV) for a single layer of Fe on 3 layers of Ir(111), in very good agreement with Ref. [22], showing that the calculation technique used, with large angles between neighbors, is reliable at least for the systems considered. The DMI we find for Co/Ir (−0.22 meV) is also of clockwise chirality but smaller than Fe/Ir (Fig. 2). The difference between Co/Ir and Fe/Ir cannot be explained by simple arguments and requires further analysis. The finding of opposite chiralities for Pt and Ir in contact with Co leads to the interesting prediction of additive effects and large DMI when Co is between Pt and Ir [47].

To sum up, we have used first principles calculations with constrained moments to determine the DMI in Co/Pt bilayers and cleared up its physical mechanism. Our main conclusion is that the large anticlockwise DMI of the bilayers [$\sim$3 mJ/m^2 for Pt(3)/Co(3)] has a predominant contribution from pair couplings between the spins of the interfacial Co layer. This DMI between the interface Co spins is directly related to the change of the SOC energy in the interface Pt atoms when the Co spin chirality is reversed. The DMI does not extend significantly into other Co layers and is very weak between the proximity-induced spins in Pt. We have also shown that the DMI of the Co/Pt bilayers is not related to the existence of proximity-induced magnetism in Pt. Our similar calculations of DMI for the Fe/Ir system are in agreement with previous *ab initio* calculations. The smaller DMIs we find for Co/Pd and Co/Au can be explained by the smaller SOC of the d states in Pd and the absence of d states at the Fermi level in Au, respectively.

The authors thank P. M. Levy, I. M. Miron, O. Boulle, L. Buda-Prejbeanu, and G. Gaudin for fruitful discussions. This work was supported by the ANR SOSPIN, ESPERADO and ULTRASKY projects, by a CNRS post-doctoral fellowship, and used HPC resources from CEA/Grenoble and GENCI-CINES (Grants No. 2012 and No. 2013-096971).

[1] I. M. Miron *et al.*, Nat. Mater. **10**, 419 (2011).
[2] S. S. P. Parkin, M. Hayashi, and L. Thomas, Science **320**, 190 (2008).
[3] K.-W. Kim, S.-M. Seo, J. Ryu, K.-J. Lee, and H.-W. Lee, Phys. Rev. B **85**, 180404 (2012).

[4] I. M. Miron, K. Garello, G. Gaudin, P.-J. Zermatten, M. V. Costache, S. Auffret, S. Bandiera, B. Rodmacq, A. Schuhl, and P. Gambardella, Nature (London) **476**, 189 (2011).

[5] K. Garello, I. M. Miron, C. O. Avci, F. Freimuth, Y. Mokrousov, S. Blügel, S. Auffret, O. Boulle, G. Gaudin, and P. Gambardella, Nat. Nanotechnol. **8**, 587 (2013).

[6] L. Liu, C.-F. Pai, Y. Li, H. W. Tseng, D. C. Ralph, and R. A. Buhrman, Science **336**, 555 (2012).

[7] J. E. Hirsch, Phys. Rev. Lett. **83**, 1834 (1999).

[8] A. Thiaville, S. Rohart, E. Jué, V. Cros, and A. Fert, Europhys. Lett. **100**, 57002 (2012).

[9] S. Emori, U. Bauer, S.-M. Ahn, E. Martinez, and G. S. Beach, Nat. Mater. **12**, 611 (2013).

[10] K.-S. Ryu, L. Thomas, S.-H. Yang, and S. S. P. Parkin, Nat. Nanotechnol. **8**, 527 (2013).

[11] I. E. Dzyaloshinskii, Sov. Phys. JETP **5**, 1259 (1957).

[12] T. Moriya, Phys. Rev. **120**, 91 (1960).

[13] A. Fert and P. M. Levy, Phys. Rev. Lett. **44**, 1538 (1980).

[14] M. Bode, M. Heide, K. von Bergmann, P. Ferriani, S. Heinze, G. Bihlmayer, A. Kubetzka, O. Pietzsch, S. Blügel, and R. Wiesendanger, Nature (London) **447**, 190 (2007).

[15] M. Heide, G. Bihlmayer, and S. Blügel, Phys. Rev. B **78**, 140403 (2008).

[16] M. Heide, G. Bihlmayer, and S. Blügel, Physica (Amsterdam) **404B**, 2678 (2009).

[17] J. Honolka, T. Y. Lee, K. Kuhnke *et al.*, Phys. Rev. Lett. **102**, 067207 (2009).

[18] F. Freimuth, S. Blügel, and Y. Mokrousov, J. Phys. Condens. Matter **26**, 104202 (2014).

[19] U. K. Roessler, A. N. Bogdanov, and C. Pfleiderer, Nature (London) **442**, 797 (2006).

[20] S. Mühlbauer, B. Binz, F. Jonietz, C. Pfleiderer, A. Rosch, A. Neubauer, R. Georgii, and P. Böni, Science **323**, 915 (2009).

[21] X. Z. Yu, Y. Onose, N. Kanazawa, J. H. Park, J. H. Han, Y. Matsui, N. Nagaosa, and Y. Tokura, Nature (London) **465**, 901 (2010).

[22] S. Heinze, K. von Bergmann, M. Menzel, J. Brede, A. Kubetzka, R. Wiesendanger, G. Bihlmayer, and S. Blügel, Nat. Phys. **7**, 713 (2011).

[23] Y. Yoshida, S. Schröder, P. Ferriani, D. Serrate, A. Kubetzka, K. von Bergmann, S. Heinze, and R. Wiesendanger, Phys. Rev. Lett. **108**, 087205 (2012).

[24] B. Dupé, M. Hoffmann, C. Paillard, and S. Heinze, Nat. Commun. **5**, 4030 (2014).

[25] E. Simon, K. Palotás, L. Rózsa, L. Udvardi, and L. Szunyogh, Phys. Rev. B **90**, 094410 (2014).

[26] G. Chen, T. Ma, A. T. N'Diaye, H. Kwon, C. Won, Y. Wu, and A. K. Schmid, Nat. Commun. **4**, 2671 (2013).

[27] S.-G. Je, D.-H. Kim, S.-C. Yoo, B.-C. Min, K.-J. Lee, and S.-B. Choe, Phys. Rev. B **88**, 214401 (2013).

[28] S. Emori, E. Martinez, K.-J. Lee, H.-W. Lee, U. Bauer, S.-M. Ahn, P. Agrawal, D. C. Bono, and G. S. D. Beach, Phys. Rev. B **90**, 184427 (2014).

[29] A. Hrabec, N. A. Porter, A. Wells, M. J. Benitez, G. Burnell, S. McVitie, D. McGrouther, T. A. Moore, and C. H. Marrows, Phys. Rev. B **90**, 020402 (2014).

[30] J. Torrejon, J. Kim, J. Sinha, S. Mitani, M. Hayashi, M. Yamanouchi, and H. Ohno, Nat. Commun. **5**, 4655 (2014).

[31] S. Pizzini, J. Vogel, S. Rohart, L. D. Buda-Prejbeanu, E. Jué, O. Boulle, I. M. Miron, C. K. Safeer, S. Auffret, G. Gaudin, and A. Thiaville, Phys. Rev. Lett. **113**, 047203 (2014).

[32] R. Lavrijsen, D. M. F. Hartmann, A. van den Brink, Y. Yin, B. Barcones, R. A. Duine, M. A. Verheijen, H. J. M. Swagten, and B. Koopmans, Phys. Rev. B **91**, 104414 (2015).

[33] J.-H. Moon, S.-M. Seo, K.-J. Lee, K.-W. Kim, J. Ryu, H.-W. Lee, R. D. McMichael, and M. D. Stiles, Phys. Rev. B **88**, 184404 (2013).

[34] K. Di, V. L. Zhang, H. S. Lim, S. C. Ng, M. H. Kuok, J. Yu, J. Yoon, X. Qiu, and H. Yang, Phys. Rev. Lett. **114**, 047201 (2015).

[35] M. Belmeguenai, J.-P. Adam, Y. Roussigné, S. Eimer, T. Devolder, J.-V. Kim, S. M. Cherif, A. Stashkevich, and A. Thiaville, Phys. Rev. **91**, 180405(R) (2015).

[36] J. H. Yang, Z. L. Li, X. Z. Lu, M.-H. Whangbo, S.-H. Wei, X. G. Gong, and H. J. Xiang, Phys. Rev. Lett. **109**, 107203 (2012).

[37] B. Zimmermann, M. Heide, G. Bihlmayer, and S. Blügel, Phys. Rev. B **90**, 115427 (2014).

[38] K.-S. Ryu, S.-H. Yang, L. Thomas, and S. S. P. Parkin, Nat. Commun. **5**, 3910 (2014).

[39] See Supplemental Material at http://link.aps.org/supplemental/10.1103/PhysRevLett.115.267210 for details of the approach as well as other supporting information.

[40] A. Fert, V. Cros, and J. Sampaio, Nat. Nanotechnol. **8**, 152 (2013).

[41] J. Sampaio, V. Cros, S. Rohart, A. Thiaville, and A. Fert, Nat. Nanotechnol. **8**, 839 (2013).

[42] J. Iwasaki, M. Mochizuki, and N. Nagaosa, Nat. Nanotechnol. **8**, 742 (2013).

[43] G. Kresse and J. Hafner, Phys. Rev. B **47**, 558 (1993).

[44] G. Kresse and J. Furthmüller, Phys. Rev. B **54**, 11169 (1996).

[45] H. J. Xiang, E. J. Kan, S.-H. Wei, M.-H. Whangbo, and X. G. Gong, Phys. Rev. B **84**, 224429 (2011).

[46] Similar approach based on orbital and site resolved SOC energy contributions was applied for interfacial magnetic anisotropy studies by A. Hallal, H. X. Yang, B. Dieny, and M. Chshiev, Phys. Rev. B **88**, 184423 (2013).

[47] H. X. Yang, O. Boulle, V. Cros, A. Fert, and M. Chshiev (to be published).